Finite Temperature Behavior of $H^+(H_2O)_6$ and $H^+(H_2O)_8$†

R. A. Christie and K. D. Jordan*

Department of Chemistry and Center for Materials and Molecular Simulation, University of Pittsburgh, Pittsburgh, Pennsylvania 15260

Received: April 4, 2002; In Final Form: May 31, 2002

The finite temperature behavior of $H^+(H_2O)_6$ and $H^+(H_2O)_8$ is investigated by means of parallel tempering Monte Carlo simulations in conjunction with the multistate empirical valence-bond method for describing the interactions. The temperature dependence of the constant volume configurational heat capacity, $C_V(T)$, of $H^+(H_2O)_8$ reveals two sharp transitions, whereas that of $H^+(H_2O)_6$ is devoid of sharp structure.

I. Introduction

In recent years considerable progress has been made in the characterization of neutral and charged water clusters. Recent experimental studies have revealed that "hot" clusters can have markedly different properties than "cold" clusters because of the much wider range of configurations explored in the former.[1−4] However, to date, there have been very few experiments on water cluster systems providing information on the properties as a function of temperature. Computer simulations are especially valuable for filling this void. Most noteworthy are simulations showing that some of the neutral clusters, for example, $(H_2O)_8$, undergo relatively sharp melting transitions.[5−12] Far less is known about the finite temperature properties of $(H_2O)_n^+$, $H^+(H_2O)_n$, and $(H_2O)_n^-$ clusters.

In this study, the parallel tempering canonical Monte Carlo simulation method[13] is used to characterize the $H^+(H_2O)_6$ and $H^+(H_2O)_8$ clusters as a function of temperature. These two clusters are chosen for investigation because of the contrasting thermal behavior of the corresponding neutral clusters, $(H_2O)_6$ and $(H_2O)_8$. Whereas numerous research groups have concluded that $(H_2O)_8$ undergoes a pronounced solid-like to liquid-like transition,[5−12] there are conflicting reports concerning $(H_2O)_6$, with the most recent studies indicating that the small peak in the calculated heat capacity of this system should not be viewed as indicative of "melting".[11,12] Because the introduction of the proton drastically alters the potential energy surface of small water clusters, large changes are expected in the thermodynamic properties as well in going from the neutral to the protonated clusters.

The nature of the solvated proton, both in small water clusters and in bulk liquid water has long been the subject of considerable speculation. Both the Eigen[14] $H_9O_4^+$ and Zundel[15] $H_5O_2^+$ species have been proposed as the fundamental "carrier" of the proton, and $H_5O_2^+$ is a key species in the Grotthuss mechanism[16] of proton mobility in bulk water. Ab initio simulations[17] with classical nuclear dynamics predict that a proton in bulk water at 300 K spends about 60% of the time as $H_9O_4^+$ and 40% as $H_5O_2^+$. Simulations with quantum mechanical treatment of the nuclear motion (through a path integral method) yield a qualitatively similar picture, with both $H_5O_2^+$ and $H_9O_4^+$ proton-bearing entities found to be important.[18]

Recently, Jiang et al.[19] have determined OH stretch spectra for $H^+(H_2O)_n$, $n = 5-8$, at a temperature of 170 ± 20 K. Comparison of the measured and calculated IR spectra enabled these researchers to assign the structures responsible for the observed spectra. This study provided direct experimental evidence of the Zundel-type $H_5O_2^+$ species.

In recent years, several simulations have been carried out with the aim of understanding the structural and thermal properties of protonated water clusters. These include canonical Monte Carlo simulations of $H^+(H_2O)_n$ ($n = 9$, 21, 40) by Svanberg and Pettersson[20] and grand canonical Monte Carlo simulations of variously sized protonated water clusters by Shevkunov and Vegiri[21] and by Kusaka and Oxtoby.[22] Singer et al.[23] studied the thermal and structural properties of $H^+(H_2O)_8$ and $H^+(H_2O)_{16}$ by means of J-walking[24] canonical Monte Carlo simulations. However, none of these studies can be viewed as definitive, either because the model potentials employed restricted the proton to a specific H_3O^+ entity or because the simulations were not run long enough to ensure equilibrium. The calculations reported in the present study are timely in that they will provide, for $H^+(H_2O)_6$ and $H^+(H_2O)_8$, information on the relative importance of $H_9O_4^+$ and $H_5O_2^+$ proton-bearing entities as a function of temperature and will examine whether these clusters undergo melting-type behavior.

II. Methodology

Simulations of the $(H_2O)_n$, $n \geq 8$, clusters have been found to be prone to quasi-ergodic behavior due to the existence of large potential energy barriers separating low-energy local minima.[25,26] Quasi-ergodic behavior is also expected to be a problem in simulations of $H^+(H_2O)_n$ clusters. To overcome this problem, the parallel tempering Monte Carlo simulation method[13] is employed. In this approach, Monte Carlo simulations are carried out in parallel for a grid of temperatures, with the highest temperature (T_1) being chosen so that the barriers in the potential energy surface are readily overcome. Most of the attempted moves are carried out using the Metropolis algorithm,[27] with the remainder involving jumps between configurations generated at different temperatures. The acceptance probability of the jump moves is given by

$$\mathrm{acc}(\vec{r}_n \rightarrow \vec{r}_{n'}) = \min\{1, \exp[-(\beta_n - \beta_{n'})(U(\vec{r}_{n'}) - U(\vec{r}_n))]\} \quad (1)$$

where $\vec{r}_n$ and $\vec{r}_{n'}$ denote the two configurations from the simulations at temperatures T_n and $T_{n'}$, respectively, and β_n and

† Part of the special issue "John C. Tully Festschrift".

10.1021/jp0209042 CCC: $22.00
Published on Web 06/27/2002

$\beta_{n'}$ represent the inverse temperatures. The energies of the configurations $U(\vec{r}_n)$ are calculated using the multistate empirical valence-bond (MSEVB) method of Schmitt and Voth.[28] The MSEVB potential is based upon a flexible, reparametrized TIP3P[29] model to represent the $H_2O\cdots H_2O$ interactions and an effective valence-bond treatment of the $H_3O^+\cdots H_2O$ interactions. The diagonal elements in the MSEVB Hamiltonian give the energies of the various valence-bond configurations with the excess proton associated with specific water molecules, and the off-diagonal matrix elements give the couplings between the valence-bond configurations. With the MSEVB model, the excess proton can be localized in either Eigen or Zundel structures and proton transfer can occur between water molecules during the course of the simulation.

In this work, the parallel tempering simulations employed 32 temperatures ranging from 5 to 240 K for $H^+(H_2O)_6$ and from 10 to 395 K for $H^+(H_2O)_8$. The simulation temperatures were determined "trial by error", with the highest temperature being chosen so that the barriers are readily surmounted, and the intermediate temperatures being chosen so that there is significant overlap between the potential energy distributions generated at adjacent temperatures. For $H^+(H_2O)_6$ this led to 2−3 K temperature intervals for the simulations carried out at low temperatures ($T \leq 20$ K), 5 K intervals for $T = 20-70$ K, 10 K intervals for $T = 70-220$ K, and a final temperature of 240 K. For $H^+(H_2O)_8$, a 5 K temperature interval was used for $T = 20-70$ K, a 10 K temperature interval for $T = 70-170$ K, a 20 K interval for $T = 170-270$ K, and a 25 K interval for $T = 270-370$ K. In this case, simulation temperatures of 10, 20, and 395 K were also included. Exchanges were attempted only between configurations sampled at adjacent temperatures, with one attempted exchange being made every 10th Monte Carlo cycle. A constraining sphere of 12 Å was used to prevent evaporative events.

Each Monte Carlo cycle consisted of an attempted rotation and translation of each molecule (both H_3O^+ and the solvating water molecules). Every fifth Monte Carlo cycle, translations of every atom in the cluster were attempted in addition to the rigid molecule moves. The step sizes were adjusted to keep the acceptance rates near 45%. The identification of the H_3O^+ entity was accomplished by analysis of the MSEVB wave function. Of course, Zundel-like structures have two valence-bond configurations of nearly equal weight, and this approach singles out the one with the slightly larger weight in the wave function for rotation and translation of a H_3O^+ entity. In principle, both dominant valence-bond structures should be used in generating the moves in such cases. However, the approach used should not introduce a bias into the simulations because the atom moves should compensate for the deficiencies of this partitioning scheme.

For each sized cluster, the parallel tempering simulations were carried out starting from two different initial configurations selected at random from configurations sampled in preliminary Metropolis Monte Carlo simulations carried out at elevated temperatures. The thermodynamic properties are found to be independent of the choice of initial configuration, thereby establishing that convergence has been achieved.

The simulations of $H^+(H_2O)_6$ employed 1×10^7 cycles for equilibration, followed by 2×10^7 cycles to collect ensemble averages, whereas those of $H^+(H_2O)_8$ employed 4×10^7 cycles for equilibration, followed by 4×10^7 production cycles. As noted above, each cycle consists of multiple attempted moves. These simulations employ far more Monte Carlo steps than previous simulations of protonated water clusters. At each temperature in the parallel tempering simulations, 10^4 configurations (one every 2000 cycles for $H^+(H_2O)_6$ and one every 4000 cycles for $H^+(H_2O)_8$) were saved for subsequent analysis. The saved configurations were optimized to their inherent structures using the steepest descent method. The various local minima were distinguished and characterized according to their hydrogen-bonding topologies.

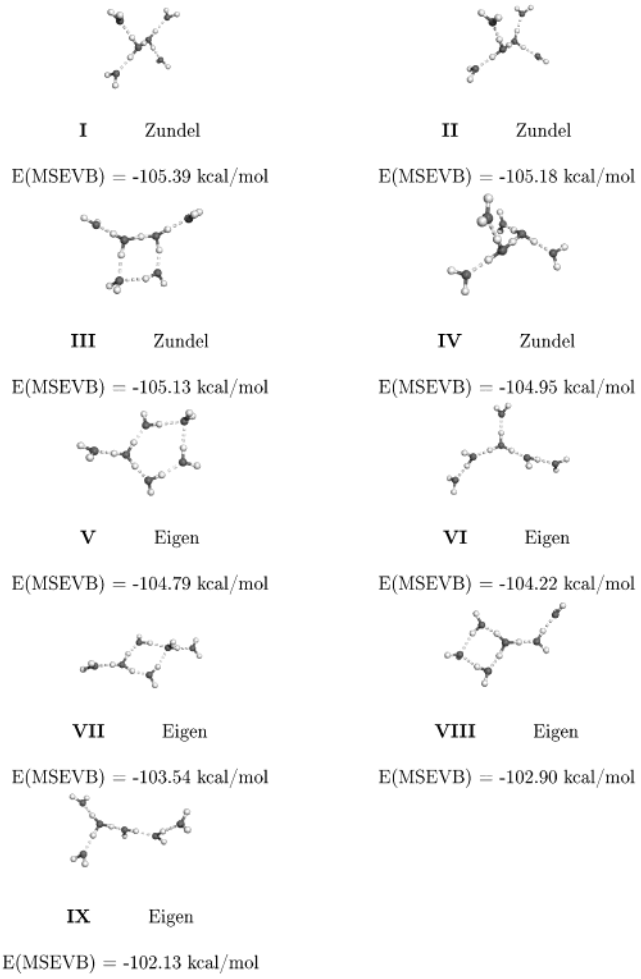

Figure 1. The nine most populated potential energy minima of $H^+(H_2O)_6$, together with their binding energies, recovered from parallel tempering Monte Carlo simulation trajectories. These are obtained by optimizing structures sampled at each of the 32 simulation temperatures. The structures are classified as Zundel-type $H_5O_2^+$, Eigen-type $H_9O_4^+$, or intermediate Zundel−Eigen depending on the weights of the various valence-bond configurations in the MSEVB wave function.

To help elucidate possible "melting" behavior of the $H^+(H_2O)_6$ and $H^+(H_2O)_8$ clusters, the dimensionless configurational constant volume heat capacity, C_V/k_B,

$$\frac{C_V}{k_B} = \frac{1}{(k_B T)^2}(\langle U(\vec{r})^2\rangle - \langle U(\vec{r})\rangle^2) \qquad (2)$$

was calculated.

III. Results and Discussion

A. $H^+(H_2O)_6$. *(i) Low-Energy Minima.* Figure 1 depicts the structures and reports the energies of the low-energy isomers of $H^+(H_2O)_6$ determined by optimizing configurations sampled in the parallel tempering Monte Carlo simulations. The various isomers are labeled as Zundel, Eigen, or Zundel−Eigen depend-

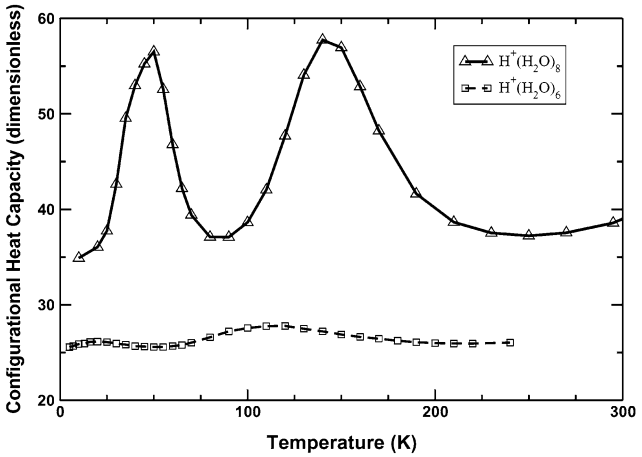

Figure 2. Temperature dependence of the constant volume configurational heat capacity, $C_V(T)$, for $H^+(H_2O)_6$ and $H^+(H_2O)_8$ from parallel tempering Monte Carlo simulations.

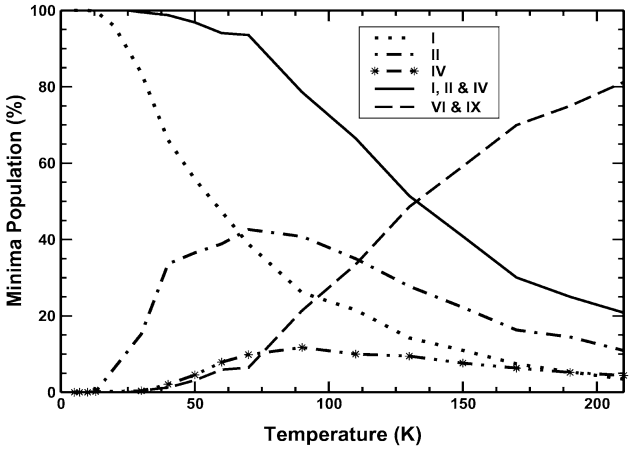

Figure 3. Temperature dependence of the population of various inherent structures of $H^+(H_2O)_6$ obtained by optimizing sampled configurations. Two distinct classes of hydrogen-bonding topology are considered, the Zundel-based minima **I**, **II**, and **IV** and the Eigen-based branched minima **VI** and **IX**.

ing on the nature of the MSEVB wave function. In those cases that the MSEVB wave function is dominated by two valence-bond configurations of nearly equal weight (i.e., to within 4%) and that together account for over 85% of the total contributions to ψ^2_{MSEVB}, the structure is designated as Zundel. In those cases that a single valence-bond configuration contributes over 60% to ψ^2_{MSEVB}, the structure is labeled as Eigen. All other structures are listed as Zundel−Eigen, indicating that there is both significant Zundel-like and significant Eigen-like character.

The lowest-energy structure located by the optimizations (minimum **I**) can be viewed as a $H_5O_2^+$ entity hydrogen bonded to four water molecules, one to each of the "free" H atoms of $H_5O_2^+$. Evidence for such a species was provided by the recent IR measurements of Jiang et al.[19] The calculations also give two minima, designated **II** and **IV**, which differ from **I** only in the orientation of the "solvent" H_2O molecules. These are calculated to lie only 0.21 (**II**) and 0.44 kcal/mol (**IV**) above **I** in energy. There is also a fourth low-lying Zundel-like structure, labeled **III**, which lies only 0.26 kcal/mol above **I** and which has a four-remembered ring (where the ring size is established by the number of oxygen atoms). The optimizations also located several other energetically higher-lying species with ring-based or branched Eigen-like structures.

Jiang et al.[19] carried out MP2/6-31+G* calculations on a select group of $H^+(H_2O)_6$ isomers and reported a structure similar to **I** as the lowest-energy minimum. The lowest-energy minima predicted in various DFT studies include a branched-type[30] structure, a structure that appears similar to **I**,[19] and a fused-ring[31] structure. The lack of agreement between the various DFT studies is likely due to differences in the basis sets and in the functionals employed. $H^+(H_2O)_6$ has also been studied[21,31,33] using the ASP,[34] Kozack−Jordan,[32] and Shevkunov−Vegiri[21] model potentials. However, each of these potentials constrains the proton to be associated with a specific H_3O^+ entity and thus does not permit proton mobility or the formation of $H_5O_2^+$-type species.

(ii) Thermal Behavior. The calculated constant volume configurational heat-capacity curve for $H^+(H_2O)_6$, shown in Figure 2, is relatively structureless over the 10−240 K temperature range examined, displaying only very weak maxima near $T = 20$ and 100 K. The populations of various inherent structures sampled over the range of simulation temperatures are shown in Figure 3. In this plot, the populations of the closely related structures **I**, **II**, and **IV** are plotted individually and grouped together. The population of the various chain structures, of which **VI**, and **IX** are the most stable, are reported as a group. The ring-based structures (**III**, **V**, **VII**, and **VIII**) do not attain a significant population over the range of temperatures explored, and their populations are not reported.

At low temperatures, only minima **I**, **II**, and **IV** are significantly populated. The net population of these species stays near 100% up to a temperature of about 30 K, after which it falls off gradually with increasing temperature, still being around 38% at $T = 200$ K. As the net population of **I**, **II**, and **IV** falls off, that of the branched minima gradually increases. From Figure 3, it is also seen that the slow fall off in the population of the **I**/**II**/**IV** group with increasing temperature is in part a consequence of the fact that **II** and **IV** grow in importance up to temperatures of about 70 and 80 K, respectively, largely compensating for the fall off in population of **I**. Near $T = 30$ K, at which the branched structures first acquire significant population, **VI**, which is the most energetically stable branched species, is far more important than **IX**. However, at high temperatures (e.g., $T \approx 210$ K), these two species are about equally populated. Neither the heat-capacity curve nor the variation in the populations of the inherent structures with temperature provides evidence for a "solid-like" to "liquid-like" transition for $H^+(H_2O)_6$.

B. $H^+(H_2O)_8$. *(i) Low-Energy Minima.* Figures 4−7 depict low-energy isomers of $H^+(H_2O)_8$ determined by optimizing configurations sampled in the parallel tempering Monte Carlo simulations. The figure also reports the energies and classifies the minima using the same scheme as that for $H^+(H_2O)_6$.

The three lowest-energy structures of $H^+(H_2O)_8$ found in the optimizations can be viewed as being derived from "cubic"-type clusters. The most stable of these, structure **A**, has the proton localized in a $H_5O_2^+$entity and differs from an "ideal" cubic topology in that the hydrogen bond diagonally opposite the $H_5O_2^+$ is broken. The other two "cubic"-derived structures, **B** and **C**, lie about 1 kcal/mol higher in energy and have a second "broken" hydrogen bond (compared to the ideal cubic structure), reducing the number of fused rings to three. **B** has a Zundel-like structure, while **C** is classified as Zundel−Eigen.

At higher energies there are numerous other local minima, including species with two fused rings (**D**−**H**), a single ring (**J**−**M**), and branched structures (**N**−**R**). The two-fused-ring isomers have Zundel or Zundel−Eigen structures, and most of the branched species are Eigen-like in nature.

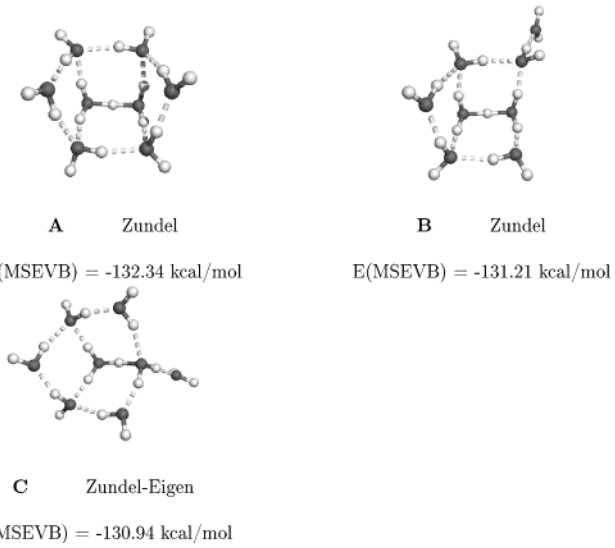

Figure 4. "Cubic"-like low-energy minima of $H^+(H_2O)_8$, together with their MSEVB binding energies. These are obtained by optimizing structures sampled at each of the 32 simulation temperatures.

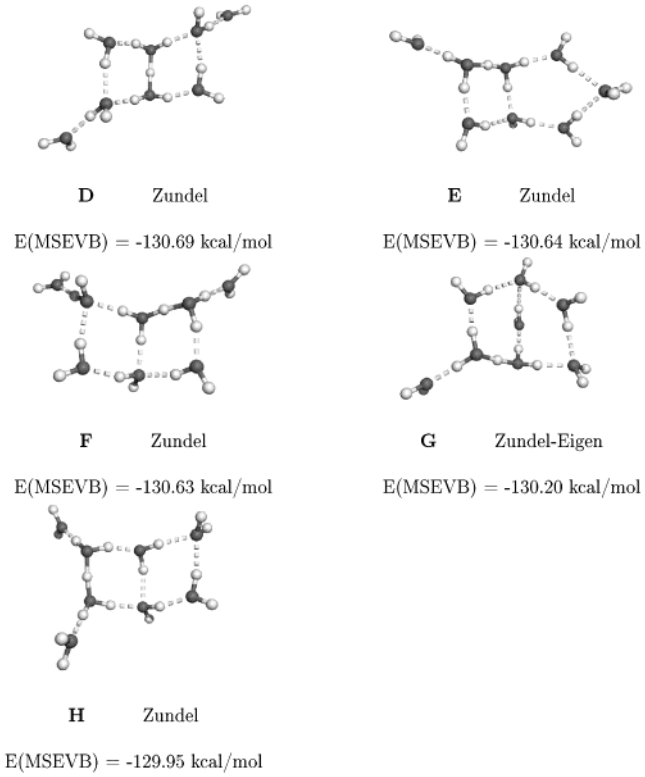

Figure 5. Five fused-ring minima of $H^+(H_2O)_8$, together with their binding energies, recovered from parallel tempering Monte Carlo simulation trajectories. These are obtained by optimizing structures sampled at each of the 32 simulation temperatures.

MP2 calculations carried out by Ciobanu et al.[36] also give "cubic"-like structures as the lowest-energy forms of $H^+(H_2O)_8$. However, the global minimum reported by these authors, unlike our species **A**, retains the hydrogen bond diagonally opposite the $H_5O_2^+$ entity. The different DFT studies do not agree on the nature of the global minimum:[19,31,38] while Hodges and Stone[31] found a "cubic"-like structure similar to that reported by Ciobanu et al.[36] as the lowest-lying minimum, Wei and Salahub[30] predicted a branched form to be the lowest-lying structure, and Jiang et al.[19] found a structure similar to **J** to be lowest in energy. $H^+(H_2O)_8$ has also been studied by Hodges

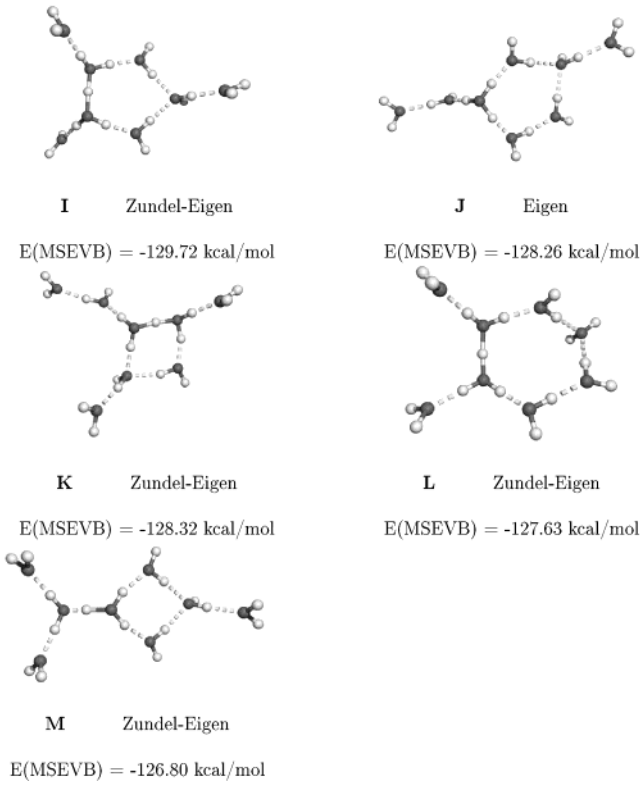

Figure 6. Five single-ring minima of $H^+(H_2O)_8$, together with their binding energies, recovered from parallel tempering Monte Carlo simulation trajectories. These are obtained by optimizing structures sampled at each of the 32 simulation temperatures.

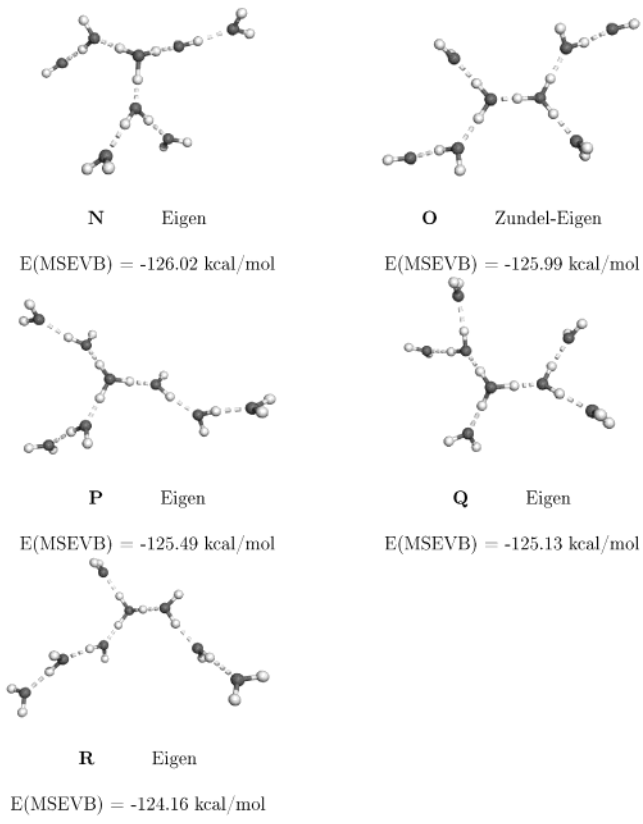

Figure 7. Five branched-type minima of $H^+(H_2O)_8$, together with their binding energies, recovered from parallel tempering Monte Carlo simulation trajectories. These are obtained by optimizing structures sampled at each of the 32 simulation temperatures.

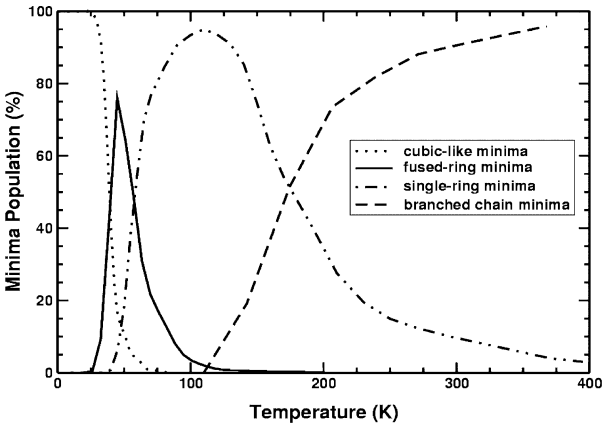

Figure 8. Variation in population of various inherent structures of $H^+(H_2O)_8$ with temperature. The "cubic"-like, fused-ring, single-ring, and branched minima correspond to the structures presented in Figures 4−7, respectively.

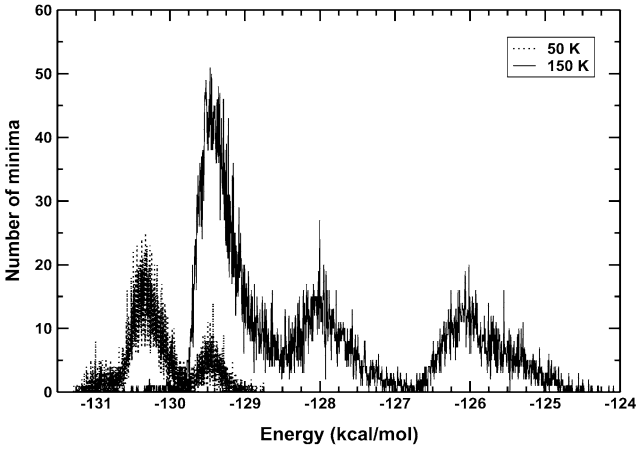

Figure 9. Histogram of $H^+(H_2O)_8$ minima energies obtained from the optimized structures recovered from trajectories of parallel tempering Monte Carlo simulations carried out at 50 and 150 K. As discussed in the text, the optimizations are not fully converged, making it appear as though there are more local minima than are actually possessed by the cluster as described by the MSEVB model.

and Stone[31] using the ASP[34] model potential, by Hodges and Wales[33] using the Kozack−Jordan[32] potential, by Shevkunov and Vegiri[21] using a potential developed by one of the authors (Shevkunov[35]), and by both Ciobanu et al.[36] and McDonald et al.[39] using the flexible OSS2[40] model potential, which allows the proton to be involved in both Zundel- and Eigen-type structures. The different model potentials differ in terms of the global minimum structure identified.

(ii) Thermal Behavior. The calculated configurational heat capacity of $H^+(H_2O)_8$ displays pronounced peaks near 50 and 145 K, with the low-temperature peak being appreciably narrower than the high-temperature peak (see Figure 2). In the vicinity of each of these two peaks, the dimensionless heat capacity undergoes a change of about 22.5.

Jump-walking[24] Monte Carlo simulations carried out by Singer et al.[23] with the OSS2 model potential[40] produced a heat-capacity plot with a single peak at $T = 165$ K with a maximum of about 18. However, these simulations were carried out for far fewer moves than those presented here and, as a result, did not achieve equilibrium (as is clear from the discussion in ref 23). Inconsistencies between the heat-capacity plots presented in ref 23 and in this study may also be due to the different model potentials employed in the respective studies.

The populations of various isomers produced in the optimizations as a function of the temperature of the simulation are reported in Figure 8. In this plot, structures have been grouped together into four classes: the "cubic"-like structures **A**−**C**, the fused-ring structures **D**−**H**, the single-ring structures **I**−**M**, and the branched-chain structures **N**−**R**. The energies of the various isomers, to a good approximation, correlate with the number of rings, going up as the number of rings decreases. As seen from Figure 8, for $T \leq 25$ K, only the cubic structures (**A**−**C**) have sizable population. As T is increased above about 25 K, the population of the cubic structures falls rapidly, being negligible for $T > 70$ K. The two-fused-ring species (**D**−**H**) first become important near $T = 25$ K, with the population having a maximum near $T = 42$ K and then falling off rapidly at still higher temperatures.

The third class of structures, those with a single ring (**I**−**M**), start to acquire sizable population near $T = 35$ K and are the most important species between 58 and 175 K. They still have a sizable population (∼4%) at the highest temperature (395 K) considered. Branched isomers do not acquire significant population until $T = 110$ K; for temperatures above $T \approx 160$ K, they are the most populated structures sampled in the simulations.

Comparison of these results with the structure in the heat-capacity plot indicates that the peak near 50 K is due primarily to a transition between the "cubic"-like structures (**A**−**C**) and both the two-ring (**D**−**H**) and single-ring (**I**−**M**) structures. The higher temperature ($T \approx 145$ K) peak arises from transitions between single-ring (**I**−**M**) and branched-chain structures (**N**−**R**).

Figure 9 presents the distributions of inherent structures sampled during the simulations carried out at $T = 50$ and 150 K, which fall near the maxima in the heat-capacity curve. Both distributions have three peaks, corresponding to three distinct sets of minima. In the 50 K simulation, the lowest-energy peak corresponds to the "cubic"-like minima, the intermediate peak to fused two-ring minima, and the highest energy peak to single-ring-type minima (especially **I**). The lowest-energy peak in the distribution generated at 150 K corresponds to the single-ring minima (especially **I**); the intermediate peak to higher energy single-ring minima (e.g., **J**−**M**), and the highest energy peak to the branched minima. It should be noted that there are actually far fewer distinct inherent structures than conveyed by this figure. The apparently larger number of distinct minima in Figure 9 is a reflection of the difficulty in fully optimizing these structures due to the existence of rather flat regions on the potential energy surface and the use of the steepest descents algorithm.

Jiang et al.[19] interpreted their IR of $H^+(H_2O)_8$ spectra in terms of minimum **I**, with a five-membered ring and the proton localized in a $H_5O_2^+$-type entity. The present simulations indicate that **I** and various branched structures have large populations at $T = 170$ K, the estimated temperature of the clusters observed experimentally.

Although the heat-capacity curve of $H^+(H_2O)_8$ displays two pronounced peaks, it is not clear that either of these should be attributed to cluster melting. Although our optimizations are not exhaustive, it does appear as though the density of local minima is relatively low over the −132.3 to −124.0 kcal/mol range. This fact, combined with the fact that the histograms of unquenched potential energies (not shown) of the configurations sampled near the two maxima (at $T = 50$ and 150 K) are not bimodal, leads us to conclude that the transitions should probably not be viewed as melting transitions.

IV. Conclusions

In this study, the parallel tempering Monte Carlo method was used to investigate the thermal behavior of $H^+(H_2O)_6$ and $H^+(H_2O)_8$. There is no pronounced structure in the $C_V(T)$ plot of $H^+(H_2O)_6$, whereas the corresponding plot for $H^+(H_2O)_8$ shows two pronounced peaks, with the low-temperature peak arising from transitions between "cubic"-like and fused-ring structures and the high-temperature peak from transitions between single-ring and branched-type minima. The local minima recovered by optimizing sampled configurations to their inherent structures reveal that the proton is found to be solvated in Zundel, Eigen, and intermediate Zundel−Eigen structures. In both $H^+(H_2O)_6$ and $H^+(H_2O)_8$, the Zundel form is preferred at low temperatures, whereas Eigen-like structures are more populated at higher temperatures.

Acknowledgment. This research was carried out with support from the National Science Foundation. The calculations were performed on computers housed in the University of Pittsburgh's Center for Molecular and Materials Simulations.

References and Notes

(1) Ayotte, P.; Weddle, G. H.; Bailey, C. G.; Johnson, M. A.; Vila, F.; Jordan K. D. *J. Chem. Phys*. **1999**, *110*, 6268.
(2) Ayotte, P.; Johnson, M. A. *J. Chem. Phys*. **1997**, *106*, 811.
(3) Jongma, R. T.; Huang, Y.; Shiming, S.; Wodkte, A. *J. Phys. Chem. A* **1998**, *102*, 8847.
(4) Brudermann, J.; Buck, U.; Buch, V. *J. Phys. Chem. A* **2002**, *106*, 453.
(5) Tsai, C. J.; Jordan, K. D. *J. Chem. Phys.* **1991**, *95*, 3850.
(6) Tsai, C. J.; Jordan, K. D. *J. Chem. Phys.* **1993**, *99*, 6957.
(7) Wales, D. J.; Ohmine, I. *J. Chem. Phys.* **1993**, *98*, 7245.
(8) Rodriguez, J.; Laria, D.; Marceca, E. J.; Estrin, D. A. *J. Chem. Phys.* **1999**, *110*, 9039.
(9) Laria, D.; Rodriguez, J.; Dellago, C.; Chandler, D. *J. Phys. Chem. A* **2001**, *105*, 2646.
(10) Nigra, P.; Carignano, M. A.; Kais, S. *J. Chem. Phys*. **2001**, *115*, 2621.
(11) Pedulla, J. M.; Jordan, K. D. *Chem. Phys.* **1998**, *239*, 593.
(12) Tharrington, A.; Jordan, K. D. Unpublished results.
(13) Neirotti, J. P.; Calvo, F.; Freeman, D. L.; Doll, J. D. *J. Chem. Phys*. **2000**, *112*, 10340.
(14) Eigen, M.; Maeyer, L. D. *Proc. R. Soc. London, Ser. A* **1958**, *247*, 505.
(15) Zundel, G.; Metzger, H. *Z. Phys. Chem. (Munich)* **1968**, *58*, 225.
(16) von Grotthuss, C. J. D. *Ann. Chim. (Paris)* **1806**, *LVIII*, 54.
(17) Tuckerman, M.; Laasonen, K.; Sprik, M.; Parinello, M. *J. Chem. Phys*. **1995**, *103*, 150.
(18) Marx, D.; Tuckerman, M. E.; Hutter, J.; Parrinello, M. *Nature* **1999**, *397*, 601.
(19) Jiang, J.-C.; Wang, Y.-S.; Chang, H.-C.; Lin, S. H.; Lee, Y. T.; Niedner-Schatteburg, G.; Chang, H.-C. *J. Am. Chem. Soc*. **2000**, *122*, 1398.
(20) Svanberg, M.; Pettersson, J. B. C. *J. Phys. Chem. A* **1998**, *102*, 1865.
(21) Shevkunov, S. V.; Vegiri, A. *J. Chem. Phys.* **1999**, *111*, 9303.
(22) Kusaka, I.; Oxtoby, D. W. *J. Chem. Phys.* **2000**, *113*, 10100.
(23) Singer, S. J.; McDonald, S.; Ojamäe, L. *J. Chem. Phys*. **2000**, *112*, 710.
(24) Frantz, D. D.; Freeman, D. L.; Doll, J. D. *J. Chem. Phys.* **1990**, *93*, 2769.
(25) Wales, D. J.; Ohmine, I. *J. Chem. Phys*. **1993**, *98*, 7257.
(26) Tsai, C. J.; Jordan, K. D. *J. Phys. Chem.* **1993**, *97*, 11227.
(27) Metropolis, N.; Rosenbluth, A. W.; Rosenbluth, M. N.; Teller, A. N.; Teller, E. *J. Chem. Phys.* **1953**, *21*, 1087.
(28) Schmitt, U. W.; Voth, G. A. *J. Chem. Phys.* **1999**, *111*, 9361.
(29) Jorgensen, W. L.; Chandrasekhar, J.; Madura, J.; Impey, R. W.; Klein, M. L. *J. Chem. Phys.* **1983**, *79*, 926.
(30) Wei, D.; Salahub, D. R. *J. Chem. Phys*. **1994**, *101*, 7633.
(31) Hodges, M. P.; Stone, A. *J. Chem. Phys*. **1999**, *110*, 7633.
(32) Kozack, R. E.; Jordan, P. C. *J. Chem. Phys.* **1992**, *96*, 3131.
(33) Hodges, M. P.; Wales, D. J. *Chem. Phys. Lett.* **2000**, *324*, 279.
(34) Stone, A. J.; Dullweber, A.; Hodges, M. P.; Popelier, P. L. A.; Wales, D. J. *ORIENT: A program for studying interactions between molecules*, version 3.2; University of Cambridge: Cambridge, U.K., 1995; available at http://fandango.chem.cam.ac.uk.
(35) Shevkunov, S. V.; Girskii, D. V. *Colloid J. (USSR)* **1998**, *60*, 104.
(36) Ciobanu, C. V.; Ojamäe, L.; Shavitt, I.; Singer, S. J. *J. Chem. Phys.* **2000**, *113*, 5321.
(37) Dunning, T. H. *J. Chem. Phys*. **1989**, *90*, 1007.
(38) Wei, D.; Salahub, D. R. *J. Chem. Phys.* **1997**, *106*, 6086.
(39) McDonald, S.; Ojamäe, L.; Singer, S. J. *J. Phys. Chem. A* **1998**, *102*, 2824.
(40) Ojamäe, L.; Shavitt, I.; Singer, S. J. *J. Chem. Phys*. **1998**, *109*, 5547.